A Basis for the Analysis of Surface Geometry of Spiral Bevel Gears*

Ronald L. Huston† and John J. Coy‡

This paper contains a summary of some geometrical procedures helpful in the fundamental studies of the surface geometry of spiral bevel gears. These procedures are based upon (1) fundamental gear geometry and kinematics as exposited by Buckingham, et al. (refs. 1 and 2), (2) formulas developed from differential geometry, and (3) geometrical concepts developed in recent papers and reports (refs. 3 to 5) on spiral bevel gear surface geometry.

Spiral bevel gears are found in virtually every transmission or gear box where power is transmitted through intersecting rotating shafts. In the majority of these transmissions, the tolerances are moderate, and thus relatively small deviations in geometrical design do not create major operating problems. However, in many cases—particularly in aircraft and helicopter transmissions—careful compliance with narrow tolerances is essential for safe and reliable performance of the gears. But, even with adherence to these narrow tolerances, the performance of the gears is, at times, unsatisfactory. This dissatisfaction has stimulated a desire for improvement in design, fabrication, and maintenance of the gears.

To attain these desired improvements, it is necessary to have a better understanding of the fundamental aspects of the kinematics, lubrication, stresses, and wear of the gears. Since gear surface geometry plays a critical role in each of these phenomena, there has recently been renewed interest by a number of investigators in studying the surface geometry. In this paper a review is presented of some recently proposed procedures for studying the surface geometry.

The emphasis of the paper is on those procedures which characterize the geometry so that the surface parametric equations, the principal radii of curvature, and the meshing kinematics are systematically determined. Initially, the focus is on theoretical, "logarithmic" spiral bevel gears as defined by Buckingham (ref. 1). These gears, however, are difficult to fabricate and are sometimes considered to be too "straight." Hence, as an alternative, most manufacturers and users have employed "circular-cut" spiral bevel gears. Therefore, the second focus of the paper is the analysis of surface characteristics of crown circular-cut gears.

Symbols

A, A'	points on a circular disk (figs. 2 to 4)
a	logarithmic spiral constant
B, B'	points on a circular disk (fig. 4)
C	involute generating circle (fig. 1); a curve defining a surface of revolution; cutter center (figs. 14 and 16)
$\mathbf{e}_i$ $(i = 1,2)$	surface base vectors (eq. (8))
g	determinant of g_{ij}
g_{ij} $(i,j = 1,2)$	metric tensor coefficients
H, V	coordinates of C (fig. 16)
$\mathbf{h}_i$ $(i = 1,2)$	fundamental vector defined by eq. (12)
h_{ij} $(i,j = 1,2)$	second fundamental tensor defined by eq. (13)
I	involute curve (figs. 1 and 8)
J	mean curvature

K	gaussian curvature
m	logarithmic spiral constant
N	normal line to a surface of revolution
N_1, N_2, N_3	mutually perpendicular unit vectors (figs. 8, 9, and 11)
N_1', N_2', N_3'	mutually perpendicular unit vectors (figs. 9 to 11)
N_φ	unit vector parallel to OP (fig. 11)
$\mathbf{n}$	a unit vector normal to a surface
$\mathbf{n}_c$	defined in fig. 12
$\mathbf{n}_r$	radial unit vector (fig. 12)
$\mathbf{n}_t$	defined in fig. 12
$\mathbf{n}_x, \mathbf{n}_y, \mathbf{n}_z$	unit vectors parallel to XYZ
O	origin of XYZ axis system (See also fig. 12.)
O'	center of involute generating circle (figs. 1 and 12); back cone apex (figs. 8 to 10)
$\hat{O}$	center of base-cone–back-cone intersection circle (figs. 2, 8, and 11)
P	typical point on a surface
P'	point of intersection of line segment $O'P$ and base-cone–back-cone intersection (figs. 1 and 11)
$\mathbf{P}$	position vector to a typical point on surface
P_m	midpoint of crown gear tooth
Q	base point of involute curve (fig. 1) and typical point on base-cone–gear-tooth intersection (figs. 8 to 11, also fig. 12.)
R	involute circle radius (fig. 1) and back-cone element length (figs. 8 and 10); radial line (fig. 8)
R_c	distance CP_m (fig. 16); cutter radius (fig. 15)
R_1, R_2	principal surface radii of curvature
r	disk radius (fig. 2) and back-cone element distance (figs. 3, 6, and 8); radius of a surface of revolution; radial distance
r_0	radius of base-cone–back-cone intersection circle (fig. 2)
S	general surface
T	tangent line to C, tangent point
u^1, u^2	surface defining parameters
X, Y, Z	mutually perpendicular coordinate-axis system
$\hat{X}, \hat{Y}, \hat{Z}$	mutually perpendicular coordinate-axis system (fig. 16)
x	length of line segment $O'P$ (fig. 1)
x, y, z	coordinates of P relative to X, Y, Z
$\hat{x}, \hat{y}, \hat{z}$	coordinates relative to X, Y, Z
α	base-cone half central angle (figs. 2, 3, 8, and 10)
α_c	back-cone half central angle (figs. 6, 10, and 11)
β	involute generating angle (fig. 1)
γ	complement to the spiral angle (fig. 7)
δ	cutout sector angle (fig. 2)
θ	angle between R and X axis; pressure angle (figs. 15 and 16); polar angle
$\hat{\theta}$	projected polar angle (figs. 9 and 11)
φ	involute generating angle (fig. 1) and central disk angle (fig. 4); angle between N and the Z axis (fig. 5); angle between n_T and the Z axis (figs. 12 and 13)
$\hat{\varphi}$	central angle in the base of a cone from a spindled disk (fig. 4) and involute angle in the base-cone–back-cone intersection (fig. 11)
ψ	inclination angle of T (fig. 5); spiral angle (figs. 9 and 16)

Preliminary Considerations

Geometrical characteristics of spiral bevel gears have been documented by the American Gear Manufacturer's Association and others (refs. 1, 2, and 6 to 12). From this documentation it is seen that spiral bevel gears (and, hence, also hypoid gears) could be considered to be at the top of a hierarchy of gears beginning with spur gears and then helical gears, straight bevel and skewed bevel gears, and finally to spiral bevel gears. In each of these gears a tooth geometry can be developed by generalizing the involute geometry commonly associated with spur gears. Therefore, for notational and other purposes, it will be helpful to briefly restate some of the fundamentals of involute curve geometry.

Involute Geometry

Consider the involute curve I (fig. 1), which for simplicity may be considered as the curve traced by the end of a cord being unwrapped around circle C. In the figure O' is the center of C, P is a typical point on I, and Q is at the base of I. The line segments QO' and PO' then form an angle φ as shown. The T is the tangent point of the tangential segment PT. The segments TO' and QO' then form the angle β. Finally, P' is the intersection point of $O'P$ and C.

If R is the circle radius, it is immediately seen that the radius of curvature ρ of I at P is

$$\rho = R\beta \tag{1}$$

Hence, in terms of β, it is easily seen that

$$x = R(1 + \beta^2)^{1/2} \tag{2}$$

and that

$$\varphi = \beta - \tan^{-1}\beta \tag{3}$$

where x is the length of the line segment $O'P$. (Eq. (2) follows immediately eq. (1), and the Pythagorean identity and eq. (3) are obtained by observing that $\tan(\beta - \varphi) = \rho/R$.)
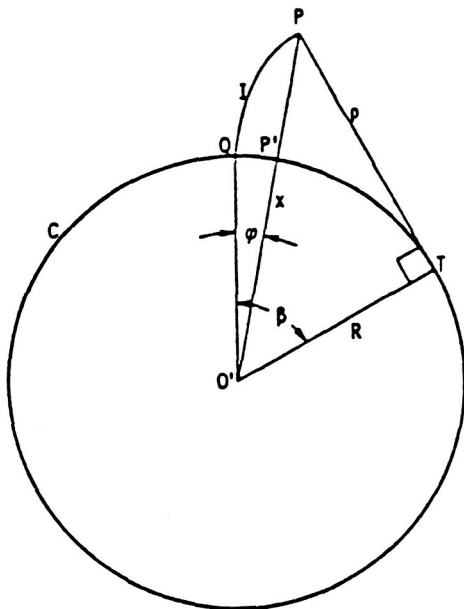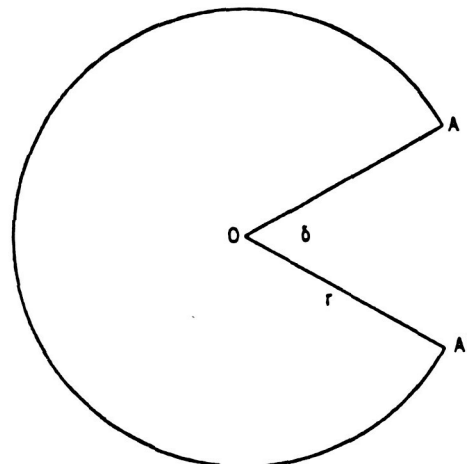

Figure 1. - Involute geometry.

Figure 2. - Circular disk with cut out sector.

Spindling a Disk into a Cone

Just as a spur can be generated by "wrapping" a basic rack into a circle, so also a bevel gear can be generated by spindling a "crown gear" (a circular disk or face gear, sometimes called a "crown rack") into a cone. Therefore, it is useful to review the geometrical aspects of spindling a disk into a cone.

Consider the disk with radius r with a cutout sector with angle φ as shown in figure 2. If points A and A' are brought together, the disk forms a cone as shown in figure 3. When r_0 is the radius at the base of the cone, it is immediately seen that

$$2\pi r_0 = (2\pi - \delta)r \qquad (4)$$

Therefore, if α is the half central angle of the cone, α and δ are related as

$$\sin \alpha = \frac{r_0}{r} = 1 - \frac{\delta}{2\pi} \qquad (5)$$

Finally, consider the disk of figure 2 with two points B and B' on the circumference. Then B and B' with O form the angle φ as shown in figure 4(a). After spindling, the top view of the resulting cone is shown in figure 4(b), where O is on the cone axis at its base. Since the arcs BB' are of equal lengths in figure 4, the angle $\hat{\varphi}$ formed by B, $\hat{O}$, and B' is then related to φ through the equation
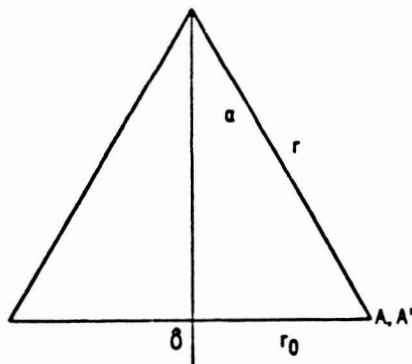

Figure 3. - Cone formed from disk of figure.

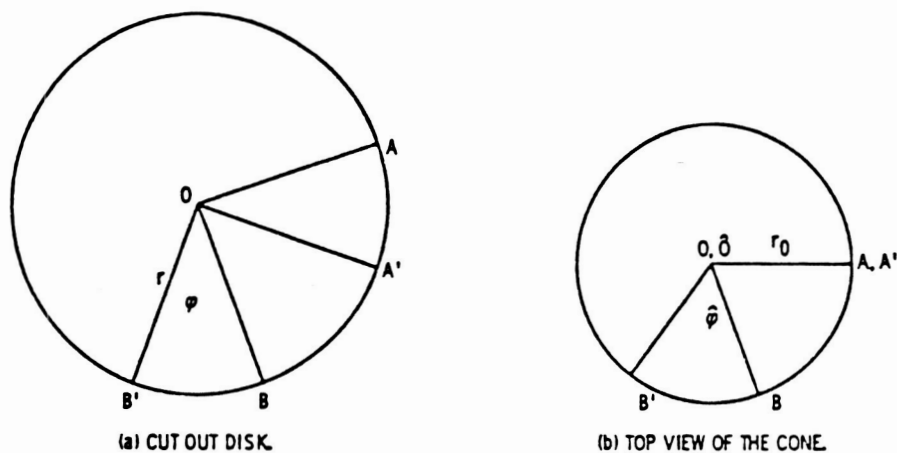(a) CUT OUT DISK   (b) TOP VIEW OF THE CONE.

Figure 4. - Disk with cut out section and top view of resulting cone.

320

$$r\varphi = r_0\hat{\varphi} \tag{6}$$

or, by using equation (5) as

$$\hat{\varphi} = \frac{\varphi}{\sin\alpha} \tag{7}$$

Differential Geometry Formulation

Major factors affecting the lubrication, surface fatigue, contact stress, wear, and life of gear teeth are the maximum and minimum radii of curvature of the tooth surface at the point of contact with the meshing tooth. To obtain the radii of curvature, it is convenient to employ some relations developed in elementary differential geometry formulations. These relations are briefly summarized here.

Suppose a surface S is described by a pair of parameters u_1 and u_2 through the vector parametric equation $\mathbf{P} = \mathbf{P}(u_1, u_2)$, where $\mathbf{P}$ is the position vector of a typical point P on S. Then base vectors $\mathbf{e}_i (i = 1,2)$ tangent to S at P are given by

$$\mathbf{e}_i = \frac{\partial \mathbf{P}}{\partial u^i} \qquad (i = 1,2) \tag{8}$$

A surface metric tensor g_{ij} $(i,j = 1,2)$ may then be defined as

$$g_{ij} = \mathbf{e}_i \cdot \mathbf{e}_j \qquad (i,j = 1,2) \tag{9}$$

Let g be det g_{ij}. Then it is easily shown that

$$\sqrt{g} = |\mathbf{e}_1 \times \mathbf{e}_2| \tag{10}$$

Hence, a unit vector $\mathbf{n}$ normal to S is given by

$$\mathbf{n} = \frac{\mathbf{e}_1 \times \mathbf{e}_2}{|\mathbf{e}_1 \times \mathbf{e}_2|} = \frac{\mathbf{e}_1 \times \mathbf{e}_2}{\sqrt{g}} \tag{11}$$

Next, let the fundamental vectors $\mathbf{h}_i (i = 1,2)$ be defined as

$$\mathbf{h}_i = \frac{\partial \mathbf{n}}{\partial u^i} \qquad (i = 1,2) \tag{12}$$

Then the second fundamental tensor h_{ij} $(i,j = 1,2)$ is defined as

$$h_{i,j} = -\mathbf{h}_i \cdot \mathbf{e}_j \qquad (i,j = 1,2) \tag{13}$$

Finally, the Gaussian curvature K and the mean curvature J are defined as

$$K = \frac{h}{g} \tag{14}$$

and

$$J = k_{ll} \tag{15}$$

where h is det h_{ij} and k_{ij} is defined as

$$k_{ij} = g_{il}^{-1} h_{ij} \tag{16}$$

where g^{-1} is the inverse tensor of g_{ij}. Regarding notation, repeated indices represent a sum (i.e., from 1 to 2) over that index.

The principal normal radii of curvature R_1 and R_2 are then easily calculated in terms of J and K as

$$R_1, R_2 = \frac{2}{[J \pm (J^2 - 4K)^{\frac{1}{2}}]} \tag{17}$$

Surfaces of Revolution

The tooth surface of a circular cut spiral bevel crown gear is a "surface of revolution;" that is, it can be developed by rotating a curve, in the shape of the cutter profile, about a fixed axis. Consider, for example, the curve C shown in figure 5. If C is rotated about the Z axis, it generates a surface of revolution S, a portion of which can be considered as the surface of a circular cut spiral bevel crown gear. Let C be defined by the expression

$$Z = f(r) \tag{18}$$

where r is the distance from the Z axis to a typical point P on C. Let φ be the angle between the Z axis and the normal line N of S at P. Then r and φ are dependent on each other; that is,

$$r = r(\varphi) \tag{19}$$

Let ψ be the inclination angle of the tangent line T to C at P as shown in figure 5. Then ψ, φ, and the slope of T are related as follows:
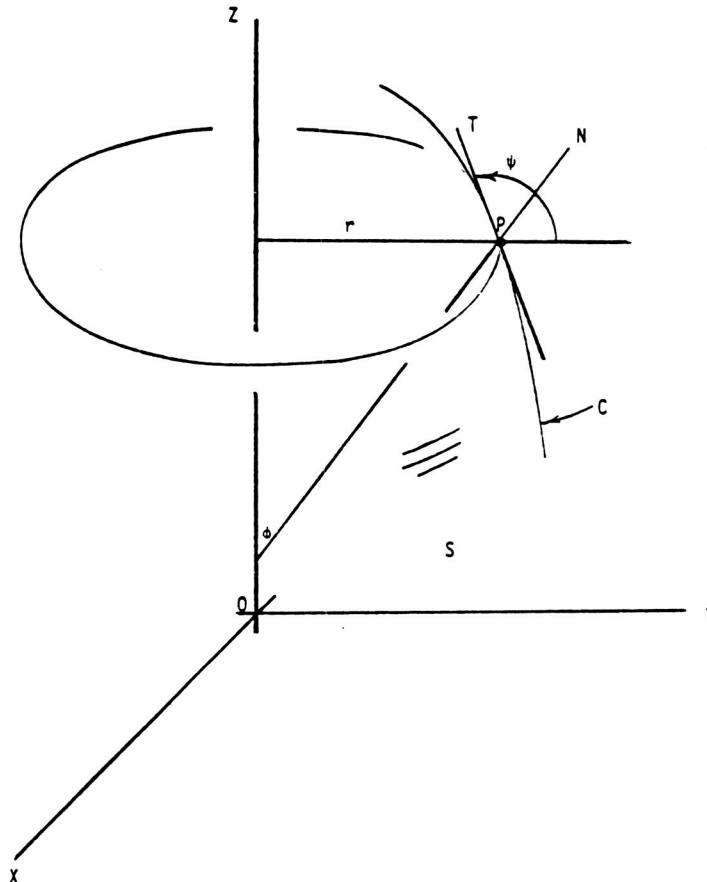

Figure 5. - A surface of revolution about the Z axis.

$$\frac{dz}{dr} = \frac{df}{dr} = -\tan \psi = +\tan(\pi - \psi) = -\tan \varphi \tag{20}$$

Consider a top view of S as shown in figure 6. In this view P is seen to lie on a circle of radius r, and on a radial line R, which makes an angle θ with the X axis. Then the position vector $\mathbf{P}$ of P relative to O, a fixed point on the Z axis (fig. 5.), is

$$\mathbf{P} = z\mathbf{n}_z + r\mathbf{n}_r = r\mathbf{n}_r + f(r)\mathbf{n}_z \tag{21}$$

where $\mathbf{n}_r$ and $\mathbf{n}_z$ are unit vectors parallel to R and the Z axis. Hence, in terms of $\mathbf{n}_x$, $\mathbf{n}_y$, and $\mathbf{n}_z$, unit vectors parallel to the X, Y, and Z axes, $\mathbf{P}$ become

$$\mathbf{P} = r \cos \theta \, \mathbf{n}_x + r \sin \theta \, \mathbf{n}_y + f(r)\mathbf{n}_z \tag{22}$$

Since $r = r(\varphi)$, P is a function of φ and θ. Therefore, it is convenient to let φ and θ be the parameters u^1 and u^2 defining S in the parametric representation $\mathbf{P} = \mathbf{P}(u^1, u^2)$ of the foregoing differential geometry formulas.

From equation (8), the surface base vectors $\mathbf{e}_1$ and $\mathbf{e}_2$ become

$$\mathbf{e}_1 - \mathbf{e}_\varphi = \left(\frac{dr}{d\varphi}\right) \cos \theta \, \mathbf{n}_x + \left(\frac{dr}{d\varphi}\right) \sin \theta \, \mathbf{n}_y + \left(\frac{df}{dr}\right)\left(\frac{dr}{d\varphi}\right) \mathbf{n}_z \tag{23}$$

and

$$\mathbf{e}_2 = \mathbf{e}_\theta = -r \sin \theta \, \mathbf{n}_x + r \cos \theta \, \mathbf{n}_y \tag{24}$$
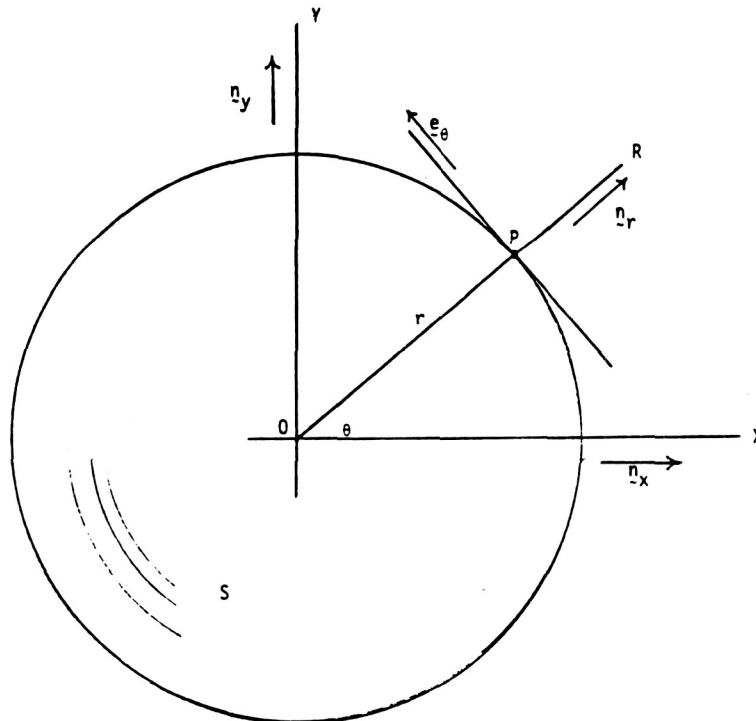

Figure 6. - Top view of surface of revolution.

Then, from equation (9) the metric tensor components become

$$g_{11} = g_{\varphi\varphi} = \left(\frac{dr}{d\varphi}\right)^2 \sec^2 \varphi \tag{25}$$

$$g_{12} = g_{21} = g_{\varphi\theta} = g_{\theta\varphi} = 0 \tag{26}$$

and

$$g_{22} = g_{\theta\theta} = r^2 \tag{27}$$

where equation (20) has been used to simplify the expressions. Hence, from equation (11) the unit vector **n** normal to S becomes

$$\mathbf{n} = \sin \varphi \cos \theta \; \mathbf{n}_x + \sin \varphi \sin \theta \; \mathbf{n}_y + \cos \varphi \; \mathbf{n}_z \tag{28}$$

The fundamental vectors $\mathbf{h}_i (i = \varphi, \theta)$ and the second fundamental tensor $h_{ij} (i,j = \varphi, \theta)$ are then

$$\mathbf{h}_1 = \mathbf{h}_\varphi = \frac{\partial \mathbf{n}}{\partial \varphi} = \cos \varphi \cos \theta \; \mathbf{n}_x + \cos \varphi \sin \theta \; \mathbf{n}_y - \sin \varphi \; \mathbf{n}_z \tag{29}$$

$$\mathbf{h}_2 = \mathbf{h}_\theta = \frac{\partial \mathbf{n}}{\partial \theta} = -\sin \varphi \sin \theta \; \mathbf{n}_x + \sin \varphi \cos \theta \; \mathbf{n}_y \tag{30}$$

$$h_{11} = h_{\varphi\varphi} = -\left(\frac{dr}{d\varphi}\right) \sec \varphi \tag{31}$$

$$h_{12} = h_{21} = h_{\varphi\theta} = h_{\theta\varphi} = 0 \tag{32}$$

and

$$h_{22} = h_{\theta\theta} = -r \sin \varphi \tag{33}$$

From equations (14) and (15) the Gaussian curvature and the mean curvature become

$$K = \frac{\sin \varphi \cos \varphi}{r \, dr/d\varphi} \tag{34}$$

and

$$J = -\left(\frac{\cos \varphi}{dr/d\varphi} + \frac{\sin \varphi}{r}\right) \tag{35}$$

Finally, using equation (17), the principal surface radii of curvature become

$$R_1 = \left| \frac{dr/d\varphi}{\cos \varphi} \right| \tag{36}$$

and

$$R_2 = \left| \frac{r}{\sin \varphi} \right| \tag{37}$$

These expressions may be expressed in terms of f by using equation (20); that is, since

$$\varphi = -\tan^{-1}\left(\frac{df}{dr}\right) \tag{38}$$

then $(d\varphi/dr)$ becomes

$$\frac{d\varphi}{dr} = -\frac{(d^2f/dr^2)}{1+(df/dr)^2} \tag{39}$$

and hence, R_1 and R_2 become

$$R_1 = \left| \frac{[1+(df/dr)^2]}{(d^2f/dr^2)\cos[\tan^{-1}(df/dr)]} \right| \tag{40}$$

and

$$R_2 = \left| \frac{r}{\sin[\tan^{-1}(df/dr)]} \right| \tag{41}$$

Theoretical Spiral Bevel Gear Tooth Surface Geometry

A Logarithmic Spiral

The name "spiral bevel" stems from the fact that, if the centerline of a crown gear tooth follows a logarithmetic spiral, the spiral angle will be constant along the tooth; that is, the tangent to the tooth centerline makes a constant angle with the radial lines. Figure 7 illustrates this where ψ_1 and ψ_2 are the angles between the tooth centerline and the radial lines at typical points P_1 and P_2. It is easily shown (ref. 13) that if the polar form of the tooth centerline equation is $r = ae^{m\theta}$, a logarithmic spiral, then $\psi_1 = \psi_2$; that is, the spiral angle is constant along the tooth. This is significant since then the complementary angles γ_1 and γ_2 are also equal and therefore constant along the tooth. This means that the tooth profile, which is normal to the radial direction, makes a constant angle with the tooth
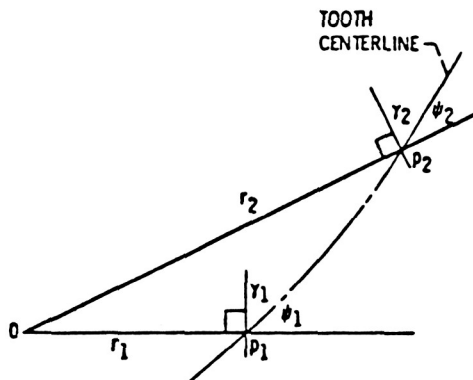
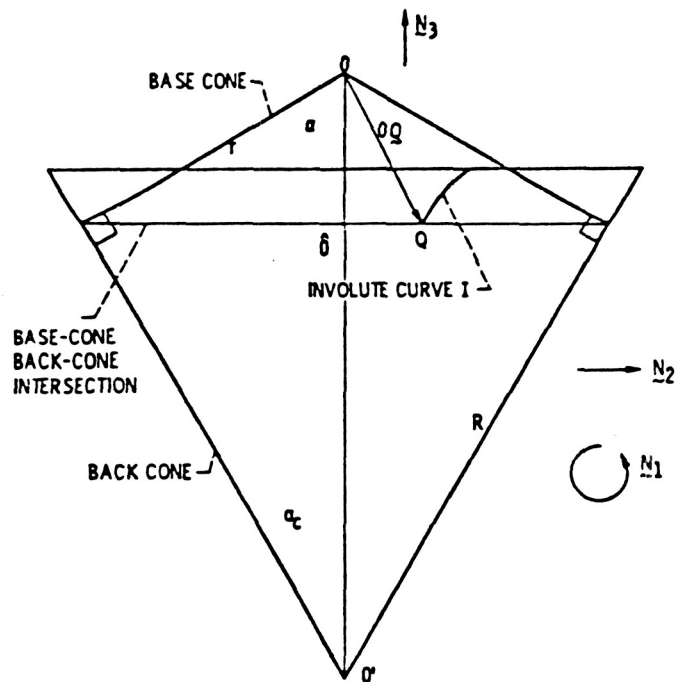Figure 7. - Radial inclination of the tooth centerline.

Figure 8. - Base cone involute spindling around a back cone.

centerline. This, in turn, is significant since it insures uniform meshing kinematics along the gear tooth with the mating gear.

The next section examines the spindling of a crown gear, with gear teeth in the shape of logarithmic spirals, into a cone.

Base Cone Geometry

To develop the geometrical basis of an ideal spiral bevel gear, imagine a crown gear with an involute tooth profile. (The tooth profile is normal to the radial direction.) Next, let this gear be spindled into a cone as described in the foregoing section. The details of this can be seen by considering figure 8 where the *base cone* and a corresponding orthogonal *back cone* of a typical gear are shown. In this figure, Q is a typical point on the base cone of a gear tooth; R is the elemental distance from the back cone apex O' to the base-cone-back-cone intersection; r is the elemental distance from the base-cone apex to the base-cone-back-cone intersection; α and α_c are the half central angles of the base and back cones, respectively (α_c is the complement of α); and N_1, N_2, and N_3 are mutually perpendicular unit vectors, with N_3 being parallel to the cone axis. Figure 8 also shows an exaggerated view of an involute curve I starting at Q and being wrapped around the base cone. Here, as in figure 1, R corresponds to the radius of the circle of the unwrapping cord which defines the involute; that is, the curve is formed by unwrapping a cord about a circle of radius R and then by spindling the resulting involute around the back cone. Finally, in figure 8 OQ is the position vector of O relative to O and its magnitude is r.

Figure 9 shows a top view of the base-cone-back-cone intersection of figure 8. Therein, θ is the angle between N_1 and the projection of OQ onto the intersection plane, and N_1', N_2', and N_3' are mutually perpendicular unit vectors, with N_3' coinciding with N_3. Figure 9 also shows the logarithmic spiral spindled about the base cone. If the logarithmic spiral is defined by $r = ae^{m\theta}$, as described in the preceding section, then $\hat{\theta}$ is related to θ by equation (7); that is,

$$\hat{\theta} = \frac{\theta}{\sin \alpha} \tag{42}$$

Position Vectors

The surface geometry of a spiral bevel gear tooth is determined once a position vector to a typical point P on the tooth surface is known. Relative to O, the base cone apex, such a position vector could take the form
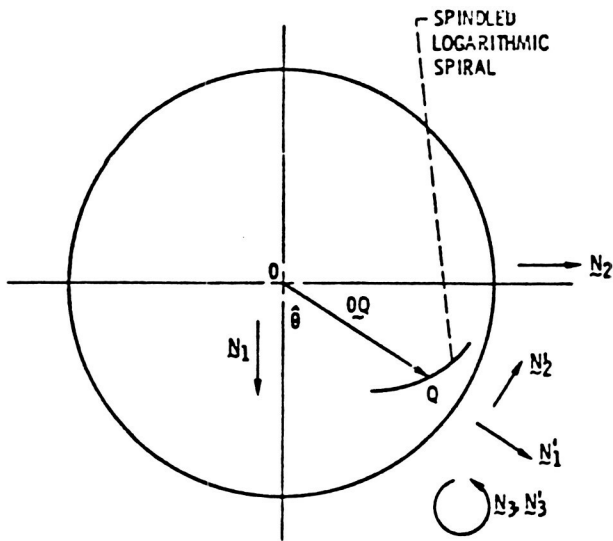

Figure 9. - Top view of base-cone - back-cone intersection and curve of a typical tooth.
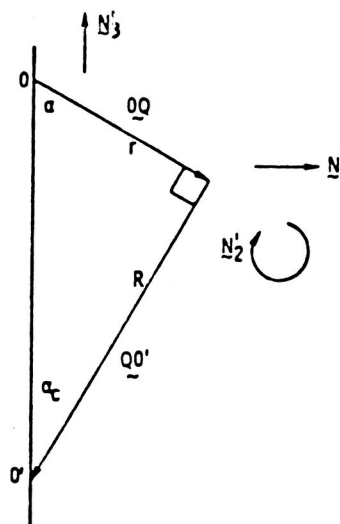

Figure 10. - True view of vectors OQ and QO'.

326

$$P = OP = OQ + QO' + O'P \tag{43}$$

where the notation is self-defining. By examining figures 8 and 9, it is readily seen that in terms of N_1, N_2, and N_3, OQ is

$$OQ = r \sin \alpha \cos \hat{\theta} \, N_1 + r \sin \alpha \sin \hat{\theta} \, N_2 - r \cos \alpha \, N_3 \tag{44}$$

Next, consider figure 10 which shows a true view of the vectors OQ and QO'. From this figure, it is immediately seen that R is equal to $r \tan \alpha$ and that QO' is then given by

$$QO' = -r \tan \alpha \cos \alpha \, N_1' - r \tan \alpha \sin \alpha \, N_3' \tag{45}$$

Finally, to determine $O'P$, note that from figure 1, $O'P$ can be written in the simple form

$$O'P = xN_\varphi \tag{46}$$

where x is given by equation (2) and where N_φ is a unit vector parallel to $O'P$ as shown in figure 11. If N_1'' is a unit vector parallel to OP' as shown, N_φ may be written as

$$N = \sin \alpha_c \, N_1'' + \cos \alpha_c \, N_3 \tag{47}$$

However, N_1'' may be expressed in terms of N_1 and N_2 as

$$N_1'' = \cos(\hat{\theta} + \hat{\varphi})N_1 + \sin(\hat{\theta} + \hat{\varphi})N_2 \tag{48}$$

where φ is the projected involute generating angle and is related to φ of figure 1 by equation (7); that is,

$$\hat{\varphi} = \frac{\varphi}{\sin \alpha_c} \tag{49}$$

Hence, from equations (46) to (48), $O'P$ becomes

$$O'P = x \sin \alpha_c \cos(\hat{\theta} + \hat{\varphi})N_1 + x \sin \alpha_c \sin(\hat{\theta} + \hat{\varphi})N_2 + x \cos \alpha_c \, N_3 \tag{50}$$
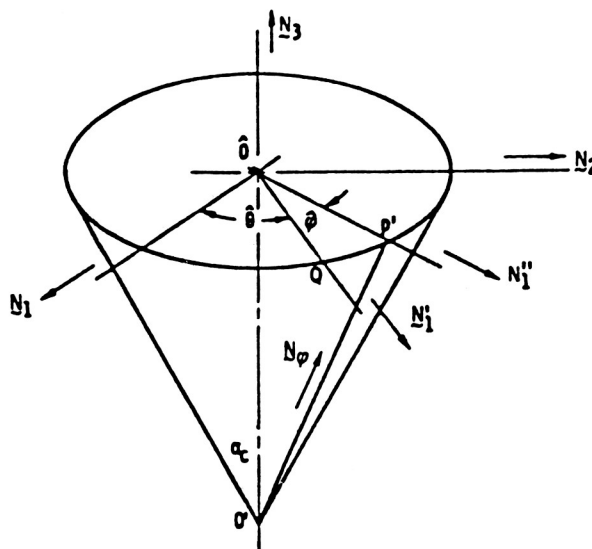

Figure 11. - Back cone unit vectors.

327

Finally, by using equations (43) to (45) and (50), **P** becomes

$$\mathbf{P} = x \sin \alpha_c \cos(\hat{\theta} + \hat{\varphi})\mathbf{N}_1 + x \sin \alpha_c \sin(\hat{\theta} + \hat{\varphi})\mathbf{N}_2 + (x \cos \alpha_c - r \sec \alpha)\mathbf{N}_3 \tag{51}$$

By noting that α and α_c are complementary (hence, $\sin \alpha_c = \cos \alpha$ and $\cos \alpha_c = \sin \alpha$) and that by equation (2) $x = r(1 + \beta^2)^{1/2} \tan \alpha$, equation (51) may be rewritten as

$$\mathbf{P} = r\left\{[(1 + \beta^2)^{1/2} \sin \alpha \cos(\hat{\theta} + \hat{\varphi})]\mathbf{N}_1 + [(1 + \beta^2)^{1/2} \sin \alpha \sin(\hat{\theta} + \hat{\varphi})]\mathbf{N}_2\right.$$

$$\left. + [(1 + \beta^2)^{1/2} \sin \alpha \tan \alpha - \sec \alpha]\mathbf{N}_3\right\} \tag{52}$$

Equation (52) can be shown to be of the form $\mathbf{P} = \mathbf{P}(u^1, u^2)$ where $u^1 = \hat{\theta}$ and $u^2 = \beta$. This is immediately seen by recalling from equations (3) and (7) that r and θ may be written as

$$r = a \exp(m\hat{\theta} \sin \alpha) \tag{53}$$

and

$$\hat{\theta} = \frac{\beta - \tan^{-1} \beta}{\cos \alpha} \tag{54}$$

If equation (28) is considered to be of the form $\mathbf{p} = \mathbf{p}(\hat{\theta}, \beta) = \mathbf{p}(u^1, u^2)$, then the differential geometry formulas of equations (8) to (17) are directly applicable. However, a glance at equations (11), (12), (16), and (17) shows that, beyond the metric tensor components, the calculation of the unit normal vector **n**, the second fundamental tensor h_{ij}, and the radii of curvature R_1 and R_2, could be quite laborious and cumbersome. Hence, they are not presented here. But, the expressions of equations (11) to (17) are in a form suitable for calculation by one of the symbolic manipulative computer languages (e.g., Formac or Macsyma). As such, the foregoing analysis provides a basis for a computerized analysis of the surface geometry of the gears.

Circular-Cut Crown Gear Tooth Surface Geometry

An Involute Curve

Although it is not practical to generate a spiral-bevel gear-tooth surface with a rotating cutter in the shape of an involute curve, it is nevertheless informative, as a first illustration, to examine the surface of revolution formed by an involute curve.

Consider the involute curve C of figure 12. The radius of curvature ρ of C at a typical point P is simply the length TP. It is easily seen that ρ is one of the principal radii of curvature of the surface of revolution, which is obtained by revolving C about the Z-axis.

To see this, consider using equations (36) and (37) of the foregoing analysis. These equations require knowledge of the radial distance r as a function of the angle. To obtain $r(\varphi)$ let O be that point on the Z axis that is at the same elevation as O', the center of the circle generating C. Then, r may be expressed as

$$r = \mathbf{n}_r \cdot \mathbf{OP} \tag{53}$$

The vector **OP** may be written as

$$\mathbf{OP} = \mathbf{OO'} + \mathbf{O'T} + \mathbf{TP} \tag{54}$$

or

$$\mathbf{OP} = b\mathbf{n}_r + a\mathbf{n}_c - a\varphi_c\mathbf{n}_t \tag{55}$$

where b is the distance OO', a is the circle radius, and φ_c is the complement of φ. In terms of $\mathbf{n}_r$ and $\mathbf{n}_z$, **OP** may be written as

$$\mathbf{OP} = \left[b - a \cos \varphi + a\left(\frac{\pi}{2} - \varphi\right) \sin \varphi \right] \mathbf{n}_r + \left[a \sin \varphi + a\left(\frac{\pi}{2} - \varphi\right) \cos \varphi \right] \mathbf{n}_z \tag{56}$$

Hence, from equation (58), r and $dr/d\varphi$ become

$$r = b - a \cos \varphi + a\left(\frac{\pi}{2} - \varphi\right) \sin \varphi \tag{57}$$

and

$$\frac{dr}{d\varphi} = a\left(\frac{\pi}{2} - \varphi\right) \cos \varphi \tag{58}$$

Therefore, from equations (36) and (37) the principal radii of curvature of the generated surface of revolution are

$$R_1 = \left| a\left(\frac{\pi}{2} - \varphi\right) \right| \tag{59}$$

and

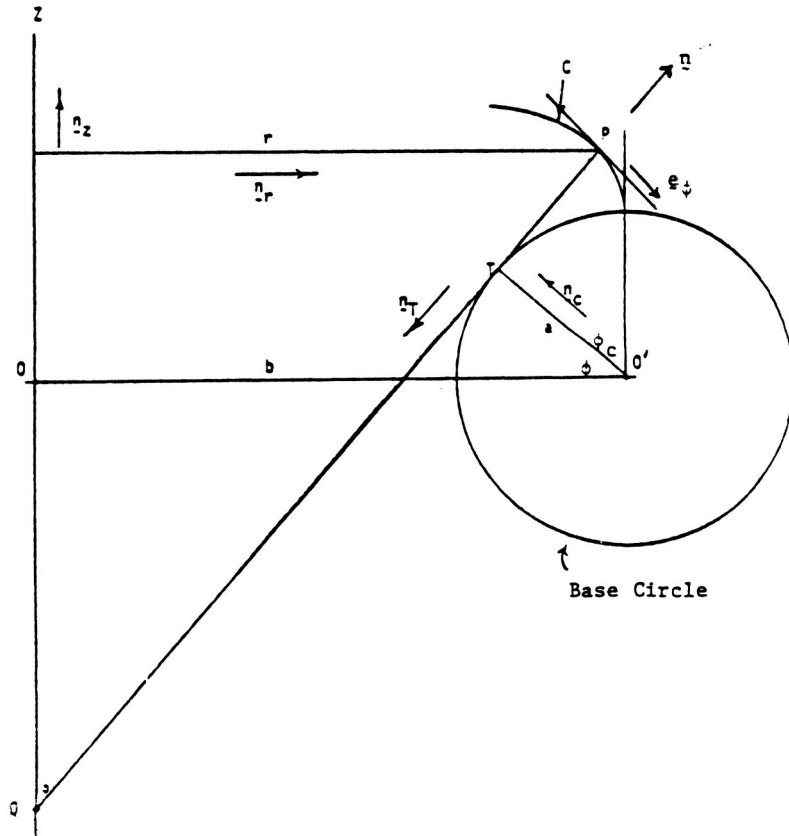$$R_2 = \left| b \csc \varphi - a \cot \varphi + a\left(\frac{\pi}{2} - \varphi\right) \right| \tag{60}$$

Figure 12. - Involute curve as generator for surface of revolution.

An examination of figure 12 shows that these expressions can be interpreted simply as

$$R_1 = |\mathbf{TP}| = R_{\min} \tag{61}$$

and

$$R_2 = |\mathbf{QP}| = R_{\max} \tag{62}$$

Finally, it is interesting to observe that, if the same analysis is carried out for an involute curve generated in the opposite direction (as shown in fig. 13) the corresponding surface of revolution has the principal radii of curvature:

$$R_1 = |\mathbf{TP}| = R_{\min} \tag{63}$$

and

$$R_2 = |\mathbf{QP}| = R_{\max} \tag{64}$$

These results are, of course, identical to equations (61) and (62). However, in this case, the centers of curvature are on opposite sides of the surface, since the Gaussian curvature is negative.

Straight Line Profile—Normal Plane

Consider next a rotating gear-tooth cutter with a straight-line profile that forms a gear-tooth surface with a straight-line profile in the normal plane as shown in figures 14 and 15. Viewed as a surface of revolution, this is a cone. Its defining equation may be expressed as
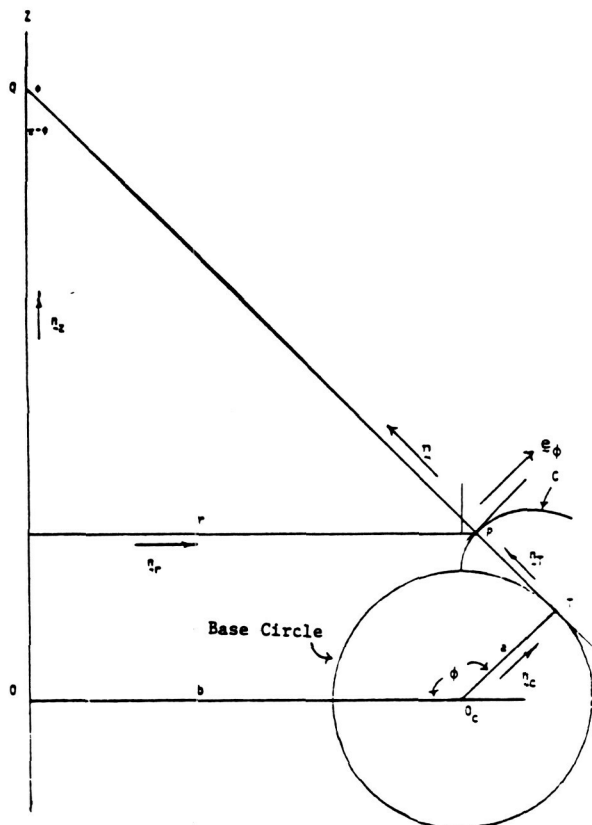

Figure 13. - Second involute curve as generator for surface of revolution.
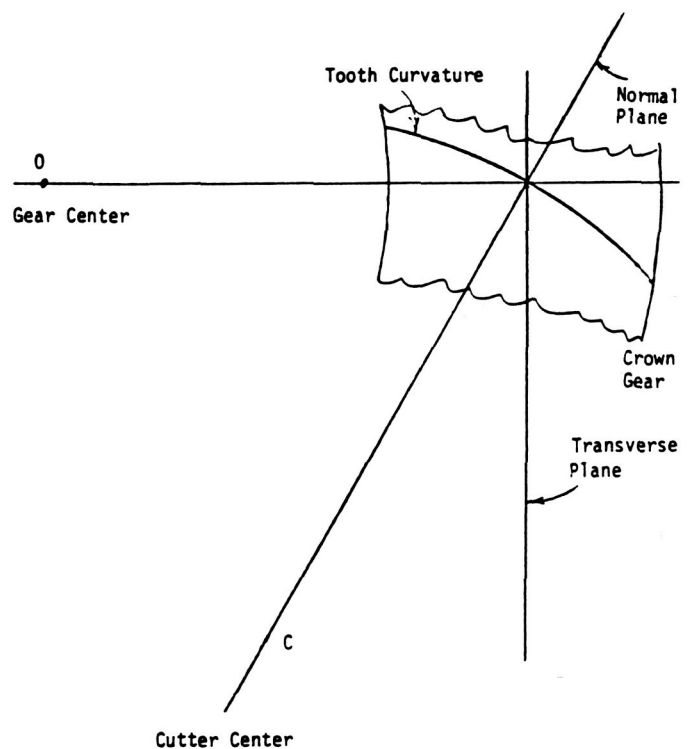

Figure 14. - Top view showing gear cutter centers and edge view of normal and transverse planes.

$$z = (r - R_c)\cot\,\theta \tag{65}$$

where θ is the pressure angle (fig. 15) and R_c is the cutter radius at the base of the tooth. From this expression dz/dr and d^2z/dr^2 are readily obtained as

$$\frac{dz}{dr} = \cot\,\theta = \tan\,\varphi \tag{66}$$

and

$$\frac{d^2z}{dr^2} = 0 \tag{67}$$

where φ is the complement of θ as shown in figure 15. Hence, equations (50) and (41) give the maximum and minimum surface radii of curvature as

$$R_{max} = \infty \tag{68}$$

and

$$R_{min} = \left| \frac{r}{\cos\,\theta} \right| \tag{69}$$

These results might also have been obtained by recalling that a cone is generated by straight-line elements (hence, infinite radius of curvature) and that the minimum radius of curvature is the distance QP as shown in figure 15.

Straight Line Profile—Transverse Plane

Finally, consider a rotating cutter which generates, for a crown gear, a straight-line meshing profile. Specifically, consider figure 16, that shows the pitch plane of a crown gear where O is the gear center and C (with X,Y coordinates H,V) is the center of the rotating cutter. Let P_m be the midpoint at the base of the gear tooth surface and let ψ be the spiral angle. The transverse plane is normal to the X axis at P_m. Since O is the gear center, the X axis is a radial line, and the intersection of the transverse plane and the gear tooth surface defines the transverse meshing profile shown in figure 17. If θ is the transverse pressure angle, the equation of the inclined tooth profile is simply
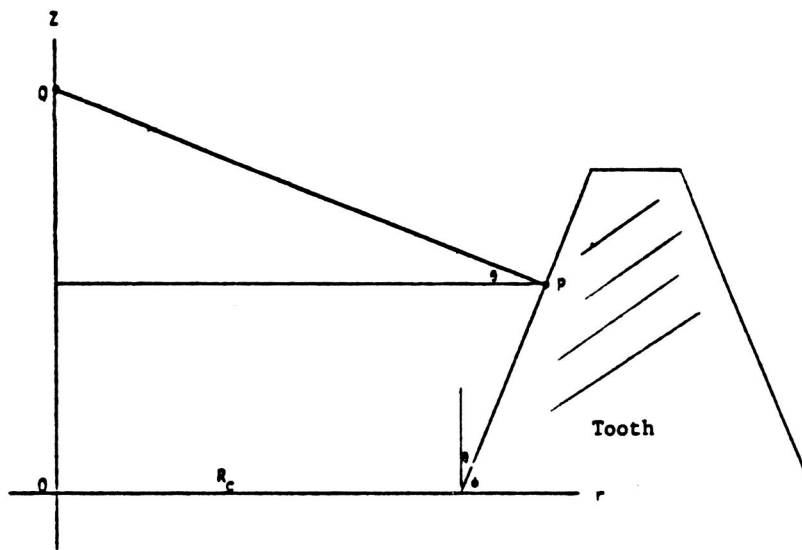
$$z = y \cot\,\theta = ky \tag{70}$$

Figure 15. - True view of normal plane showing crown tooth profile.

where z and y refer to coordinates along the Z and Y axis and k is defined as cot θ. Relative to the $\hat{X}$, $\hat{Y}$, and $\hat{Z}$ axes of figure 16, equation (70) becomes

$$z = \hat{z} = k(\hat{y} + V) \qquad (71)$$

In terms of x, y, and z, the profile of the cutter radius can be expressed in general as

$$\hat{z} = f(r) = f\left[(\hat{x}^2 + \hat{y}^2)^{1/2}\right] \qquad (72)$$

The form of f, which defines the tooth surface of revolution, may be determined by observing that the intersection of the revolution surface of the cutter with the transverse plane must coincide with the tooth profile of figure 17. If R_c is the distance between C and P_m, then the $\hat{X}$ coordinate of P_m is simply $R_c \sin \psi$. Hence, by letting $\hat{x} = R_c \sin \psi$ and by matching equations (71) and (72), the following relation is obtained:

$$f\left[(R_c^2 \sin^2 \psi + \hat{y}^2)^{1/2}\right] = k(\hat{y} + V) \qquad (73)$$

Let $\bar{r}$ be defined as

$$\bar{r} = (R_c^2 \sin^2 \psi + y^2)^{1/2} \qquad (74)$$

Then, in terms of $\bar{r}$, $\bar{y}$ becomes

$$\bar{y} = (\bar{r}^2 - R_c^2 \sin^2 \psi)^{1/2} \qquad (75)$$

where the negative root is required to be consistent with the coordinate system of figure 16. Hence, by equation (73), f is determined as

$$f(\bar{r}) = k\left[V - (\bar{r}^2 - R_c^2 \sin^2 \psi)^{1/2}\right] \qquad (76)$$

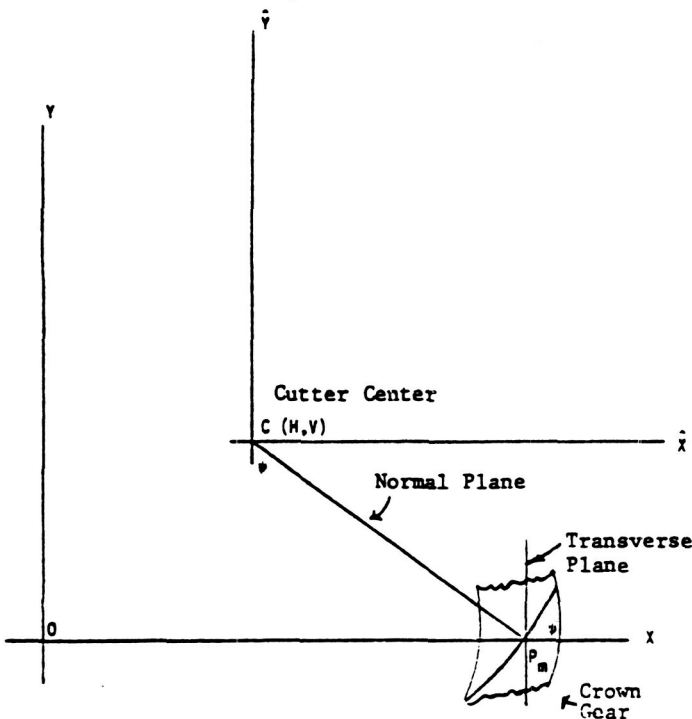which is the equation of an hyperboloid.
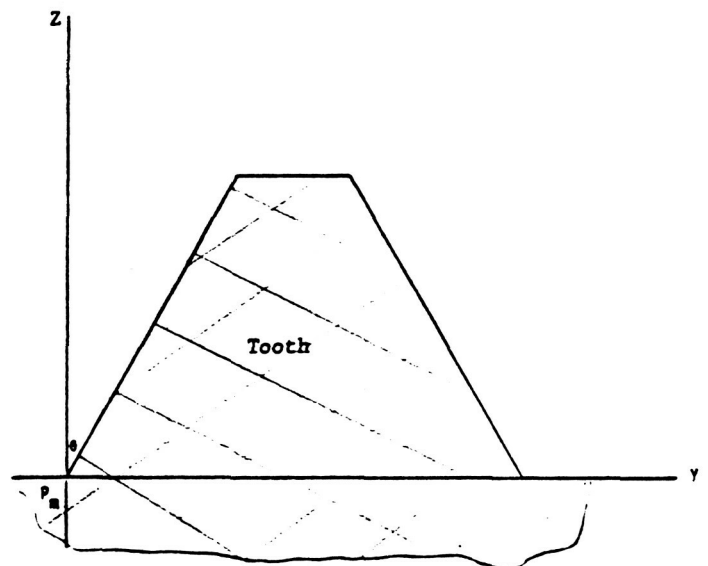

Figure 16. - View of crown gear pitch plane.

Figure 17. - True view of transverse plane showing crown tooth profile.

The maximum and minimum radii of curvature may now be determined directly by substitution into equations (40) and (41) or, alternatively, into equations (36) and (37). To do this, note that, based on equation (2), df/dr is

$$\frac{df}{dr} = -\tan \varphi = \frac{-kr}{(r^2 - R_c^2 \sin^2 \varphi)^{1/2}} \tag{77}$$

where φ is still defined as the angle between the tooth surface normal and the Z axis. Then r and $dr/d\varphi$ become

$$r = \frac{R_c \sin \psi \tan \varphi}{(\tan^2 \varphi - k^2)^{1/2}} \tag{78}$$

and

$$\frac{dr}{d\varphi} = \frac{-k^2 R_c \sin \psi \sec^2 \varphi}{(\tan^2 \varphi - k^2)^{3/2}} \tag{79}$$

Hence, on using equations (36) and (37), R_1 and R_2 become

$$R_1 = \left| \frac{k^2 R_c \sin \psi \sec^3 \varphi}{(\tan^2 \varphi - k^2)^{3/2}} \right| \tag{80}$$

and

$$R_2 = \left| \frac{R_c \sin \psi \sec \varphi}{(\tan^2 \varphi - k^2)^{1/2}} \right| \tag{81}$$

These expressions may be written in more convenient form by expressing φ in terms of z; that is, by identifying z with f in equation (76), it is readily seen that

$$r^2 = R_c^2 \sin^2 \psi + \left(\frac{kV - z}{k} \right)^2 \tag{82}$$

Then, by equation (77), $\sec^2 \varphi$ becomes

$$\sec^2 \varphi = 1 + \tan^2 \varphi = 1 + k^2 + \left(\frac{k}{kV - z} \right)^2 k^2 R_c^2 \sin^2 \psi \tag{83}$$

Hence, R_1 and R_2 may be written as

$$R_1 = \frac{\{[(kV - z)/k]^2(1 + k^2) + k^2 R_c^2 \sin^2 \psi\}^{3/2}}{kR_c^2 \sin^2 \psi} \tag{84}$$

and

$$R_2 = \frac{\{(1 + k^2)[kV - z)/k]^2 + k^2 R_c^2 \sin^2 \psi\}^{1/2}}{k} \tag{85}$$

Discussion

The basis of the foregoing exposition with theoretical spiral bevel gears is the assumption of a gear tooth having an involute profile in the transverse plane and a centerline as a logarithmic spiral. Although such gears are not convenient to manufacture, it is clear that unless the tooth centerline is a logarithmic spiral, the tooth profile, which engages the meshing gear, will not be uniform along the tooth. This could adversely modify the surface characteristics which, in turn, could affect the pressure angle, the bending stress, the contact stress, the lubrication, and the wear of the gear. Also, unless the gear tooth is spindled around the base cone, there could occur excessive sliding at the heel and toe of the tooth during meshing—particularly if the tooth is long.

The geometry of the circular-cut spiral bevel gears is somewhat simpler than that of the theoretical logarithmic spiral bevel gears. Admittedly, the restriction in the foregoing analysis to circular-cut *crown* gears contributes to the simplification. However, the modification of the foregoing expressions for conical gears can be obtained by following the procedures used for the logarithmic spiral gears.

The formulas for the radii of curvature of a surface of revolution (eqs. (36), (37), (40), and (41)) are applicable to circular-cut gear surfaces of any profile. The involute profile was used as an example because of its simplicity and because of the interesting results. It should be noted, however, that the involute profile as considered above is in the radial plane of the cutter (the normal plane of the gear) and *not* the transverse plane.

Finally, the straight-line crown profile in the transverse plane, when considered in the radial plane of the cutter, that is, the normal plane, generates a hyperboloid. Although this is a surface of revolution, it is also a "ruled surface" since it can be considered as generated by a one-parameter family of lines. Equations (84) and (71) show that the maximum radii of curvature occurs when $z = kv$ or when $y = 0$, that is, at the pitch surface. Similarly, equation (84) shows that the minimum radii of curvature occurs at the greatest elevation above the pitch surface.

Although the analysis and fabrication of circular-cut gears is considerably simpler than the theoretical logarithmic spiral gears, the apparent difference in their centerlines is relatively small. Indeed, Buckingham (ref. 1) has shown that within reasonable limits, the inclinations of the centerlines differ by less than $\pm 6°$. However, the consequences of this difference in terms of its effects on the kinematics, the stresses, the lubrication, and the wear need further study. It is believed that the analytical procedures presented herein provide a basis for such studies.

References

1. Buckingham, E.: Analytical Mechanics of Gears. Dover, New York, 1963.
2. Dudley, D. W., ed.: Gear Handbook, 1962.
3. Huston, R. L.; and Coy, J. J.: Ideal Spiral Bevel Gears—A New Approach to Surface Geometry. NASA TM-82446 and AVRADCOM 80-C-5, 1980.
4. Huston, R. L.; and Coy, J. J.: A New Approach to Surface Geometry of Spiral Bevel Gears. Part I—Ideal Gears. J. Mech. Des., vol. 103, Jan. 1981, pp. 127-133.
5. Huston, R. L.; and Coy, J. J.: Surface Geometry of Circular Cut Spiral Bevel Gear. NASA TM-82622, 1981.
6. AGMA Standard Gear Nomenclature—Terms, Definitions, Symbols and Abbreviations. AGMA Publication 112.05, 1976.
7. AGMA Reference Information–Basic Gear Geometry. AGMA Publication 115.01, 1959.
8. AGMA Standard System for Spiral Bevel Gears. AGMA Publication 209.03, 1964.
9. Dyson, A.: A General Theory of the Kinematics and Geometry of Gears in Three Dimensions. Clarendon Press, Oxford, 1969.
10. Baxter, M. L., Jr.: Exact Determination of Tooth Surfaces for Spiral-Bevel and Hypoid Gears. American Gear Manufacturers Association Semiannual Meeting, 1966. AGMA paper No. 139.02.
11. Coleman, W.: Guide to Bevel Gears. Product Engineering, vol. 34, June 10, 1963, p. 87.
12. Litvin, F. L.: Relationships Between the Curvatures of Tooth Surfaces in Three-Dimensional Gear Systems. NASA TM X-75130, 1977.
13. Schwartz, A.: Analytical Geometry and Calculus. Holt, Rinehart, and Winston, New York, 1960, p. 528.